Scientific Papers. Series E. Land Reclamation, Earth Observation & Surveying, Environmental Engineering. Vol. XV, 2026
Print ISSN 2285-6064, CD-ROM ISSN 2285-6072, Online ISSN 2393-5138, ISSN-L 2285-6064

PHOTOCHEMICAL DEGRADATION OF IMIDACLOPRID IN WATER UNDER UV RADIATION THROUGH CFD MODELING

Alexandru Florin SIMION, Angelica Nicoleta GĂMAN, Sorin SIMION, Marius KOVACS

National Institute for Research and Development in Mine Safety and Protection to Explosion – INSEMEX, Petroșani, Romania

Corresponding author email: alexandru.simion@insemex.ro

Abstract

Photochemical degradation under ultraviolet (UV) radiation is a significant transformation process that modifies pesticide concentration dynamics in aquatic environments. This study investigates the UV-induced photochemical degradation of imidacloprid in water through Computational Fluid Dynamics (CFD) modelling. Imidacloprid, a widely used agricultural insecticide, is frequently detected in surface waters, underscoring the importance of its photochemical behaviour for understanding concentration fluctuations in aquatic systems. The numerical model couples fluid flow and species transport with a UV-dependent photochemical degradation term to simulate the spatial and temporal evolution of imidacloprid concentrations. The degradation process is represented by a pseudo-first-order kinetic model, in which the reaction rate is determined solely by the local UV radiation intensity. Transient simulations were conducted to assess the influence of hydrodynamic conditions and UV exposure on the reduction in imidacloprid concentration within the flow domain. The results reveal a heterogeneous distribution of degradation rates, governed by spatial variations in flow patterns and UV intensity. This study isolates UV-induced photochemical degradation, excluding other chemical or biological transformation mechanisms, to elucidate the specific contribution of photochemical processes to pesticide concentration dynamics in aquatic environments.

Key words*: CFD modelling, imidacloprid, pesticide pollution, photochemical processes, UV radiation, water quality.*

INTRODUCTION

Global urbanisation has increased significantly in recent decades, resulting in a substantial shift of populations from rural to urban areas and a corresponding modification of demographic patterns (Gu et al., 2021). The proportion of the global population residing in urban areas rose from approximately 30% in 1950 to around 56–57% between 2020 and 2024, and is projected to reach nearly 68% by 2050 (United Nations, 2025). This demographic transition has intensified pressure on agricultural systems, prompting the expansion and intensification of crop production. Consequently, the use of agrochemicals has increased to maintain high agricultural productivity and ensure global food security (Aktar et al., 2009). Projections indicate that global food production must increase by approximately 60-70% in the coming decades, necessitating intensive farming practices, technological innovations such as precision agriculture and genetically modified organisms (GMOs), and the implementation of sustainable agricultural strategies to minimise environmental degradation (Tudi et al., 2021). Spatial heterogeneity in environmental processes, such as the non-uniform distribution of degradation rates for agrochemicals like pesticides, presents an important consideration for water-quality management. For example, identifying areas within aquatic systems that exhibit slower natural degradation could inform the strategic placement of water-quality monitoring stations or suggest optimal zones for implementing UV-enhancement interventions. Translating these model outputs into actionable guidance helps prioritise management efforts, improve the efficiency of resource allocation, and support proactive interventions in vulnerable zones.

Neonicotinoid insecticides are widely used in modern agriculture (Stehle et al., 2023). They have high efficacy against many insect pests and possess systemic properties. Imidacloprid (IUPAC name: N-[1-[(6-chloropyridin-3-yl)methyl]-4,5-dihydroimidazol-2-yl]nitramide) is one of the most common in this class. Imidacloprid acts as an agonist of nicotinic acetylcholine receptors (nAChRs) in

the insect nervous system. This causes overstimulation of neural transmission, paralysis, and death (Zhang et al., 2008). Its systemic nature enables absorption and distribution throughout plant tissues, providing broad pest protection (Simon-Delso et al., 2015; Merga & Van den Brink, 2025). These properties also contribute to its persistence and potential dispersion in the environment. Imidacloprid has relatively high water solubility (~610 mg/L at 20°C), moderate environmental persistence, and low soil sorption. These traits increase its mobility in aquatic systems (Tomizawa & Casida, 2005). As a result, imidacloprid is often detected in surface waters. This is mainly due to agricultural runoff, spray drift, soil erosion, and drainage linked to intensive farming (Peterson, 2007; Malla et al., 2021). Pesticide residues can also reach shallow groundwater by infiltrating soils in agricultural regions (Gavrilescu, 2005; Arias-Estévez et al., 2008).

The occurrence of neonicotinoid insecticides in aquatic ecosystems has raised significant environmental concerns due to their potential toxic effects on non-target organisms (Van Dijk et al., 2013; Morrissey et al., 2015). Several studies have demonstrated that neonicotinoids can impact a wide range of aquatic invertebrates and other organisms at relatively low concentrations, potentially altering trophic interactions and ecosystem functioning (Tomizawa & Casida, 2005). The toxicity of pesticides in aquatic environments is influenced by physicochemical parameters, including temperature, pH, dissolved oxygen concentration, and salinity (Klaassen et al., 1986). The magnitude of toxic effects also depends on the chemical properties of the compound, the sensitivity of exposed species, and prevailing environmental conditions (Costache & Modrogan, 2006). Therefore, the persistence, transport, and transformation of pesticides in aquatic systems are critical factors in determining their ecological impact.

In response to these potential environmental risks, pesticides present in aquatic environments are subject to strict regulation within the European Union. The Water Framework Directive (Directive 2000/60/EC) establishes a comprehensive legislative framework to achieve good ecological and chemical status for surface waters, while Directive 2013/39/EU defines environmental quality standards for priority substances and other pollutants. These regulatory frameworks underscore the importance of understanding the environmental fate and transformation mechanisms of pesticides in aquatic systems to support effective environmental monitoring and risk assessment strategies. Photochemical degradation induced by ultraviolet (UV) radiation is a significant natural attenuation mechanism for organic contaminants in surface waters (Zepp et al., 1977; Zepp et al., 1995; Schwarzenbach et al., 2010). Imidacloprid can undergo both direct photolysis, via photon absorption leading to molecular transformation, and indirect photochemical reactions mediated by reactive species, such as hydroxyl radicals, generated in aquatic environments (Wamhoff & Schneider, 1999; Lu et al., 2015). Studies have shown that the photolytic half-life of imidacloprid in aqueous systems varies considerably depending on radiation intensity, water composition, and environmental conditions, ranging from several hours to several days (Wamhoff & Schneider, 1999; Fenoll et al., 2011). The efficiency of photochemical degradation is further influenced by factors such as water depth, turbidity, dissolved organic matter, and hydrodynamic mixing conditions (Schwarzenbach et al., 2010; Fenoll et al., 2011). While the environmental occurrence, persistence, and toxicity of imidacloprid have been extensively studied (Bonmatin et al., 2015; Morrissey et al., 2015), fewer studies have examined the interactions between hydrodynamic transport processes and photochemical degradation mechanisms. In natural aquatic systems, contaminant behaviour is governed by both chemical transformation reactions and physical transport processes such as advection, dispersion, diffusion, and turbulent mixing (Fischer et al., 1979; Chapra, 1997), which determine the spatial distribution and residence time of pollutants.

Despite growing interest in pesticide photodegradation, combining UV-induced degradation with hydrodynamic modelling remains limited, especially in controlled-flow experiments.

Integrating hydrodynamic modelling with degradation kinetics is essential for predicting the fate of pesticides. Computational Fluid Dynamics (CFD) models simulate fluid flow and contaminant transport in aquatic environments (Versteeg & Malalasekera, 2007; Blocken, 2015). These models solve equations of fluid motion and mass transport. This allows coupling hydrodynamic processes with chemical kinetics and enables simulation of pollutant dispersion and degradation under controlled conditions. In this work, imidacloprid degradation follows a pseudo-first-order reaction rate. Key assumptions are: (i) the photodegradation quantum yield is constant, (ii) UV intensity is stable, (iii) scavengers and secondary reactive species are negligible, (iv) temperature and pH are constant, and (v) no intermediate products significantly affect the rate. These assumptions simplify the model and link photodegradation kinetics to measurable variables. The aim is to investigate imidacloprid's photodegradation under UV using CFD modelling.
The model combines hydrodynamic transport processes with degradation kinetics used to simulate the spatial and temporal evolution of imidacloprid concentrations in a controlled aquatic system.

MATERIALS AND METHODS

Photochemical degradation of imidacloprid in water under ultraviolet (UV) radiation was investigated. The study used a Computational Fluid Dynamics (CFD) approach implemented in ANSYS Fluent 2026 R1. The numerical model simulated the system's hydrodynamic behaviour. It also simulated the transport and transformation of imidacloprid under UV irradiation.

Computational approach

The CFD model integrates radiation transport, heat transfer, and reactive species transport. This combination allows the simulation of the photochemical degradation of imidacloprid in water. Ultraviolet radiation (280-400 nm) was modelled using the Discrete Ordinates (DO) radiation model. This model calculates radiation intensity in a participating medium. The attenuation of ultraviolet radiation within the water column was described using the Beer-Lambert law. This law accounts for exponential absorption along the optical path.
The transport and degradation of imidacloprid were simulated using the Species Transport model in ANSYS Fluent. Photochemical degradation was treated as a volumetric reaction following pseudo-first-order kinetics. The degradation rate depends on the local radiation intensity. The energy equation was included to account for thermal effects from radiation absorption. Transient simulations evaluated the time-dependent development of imidacloprid concentration during ultraviolet irradiation.

Geometry and computational domain

The computational domain models a simplified photochemical reactor to simulate ultraviolet-induced degradation of imidacloprid in water. The reactor geometry is two-dimensional, reducing computational cost while preserving key physical processes such as radiation absorption and photochemical degradation.
The computational domain has dimensions of 500 mm in length and 700 mm in height (Figure 1), representing the irradiated water volume. The aqueous phase fills the domain, where photochemical degradation of imidacloprid occurs under ultraviolet irradiation.

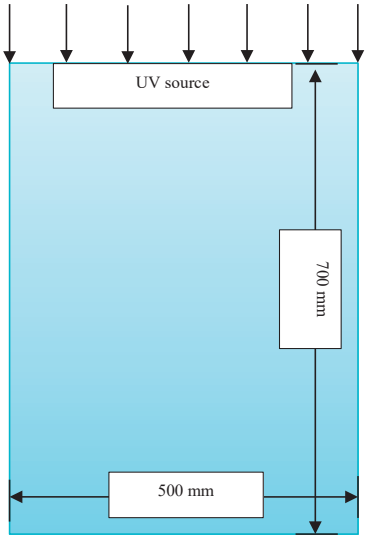


Figure 1. Computational fluid domain

Ultraviolet radiation was introduced at the upper boundary of the computational domain to represent the UV irradiation source. The radiation propagates vertically through the water column from top to bottom, simulating the penetration of ultraviolet light into the aqueous medium.

Mesh generation

The computational domain was discretised using a structured-dominant mesh generated in ANSYS Meshing. A quad-dominant meshing approach was applied to ensure numerical stability and efficiency of the two-dimensional domain (Wang et al., 2026). Mesh refinement was introduced near the UV radiation source to capture strong radiation gradients, using a bias factor of 4 in the direction of radiation penetration.

Mesh quality was evaluated using standard indicators. The skewness values ranged from 1.3057×10^{-10} to 1.3065×10^{-10}; the aspect ratio ranged from 1.0009 to 1.8218; and the orthogonal quality ranged from 0.84364 to 1, confirming the high numerical quality of the computational grid (Figure 2).

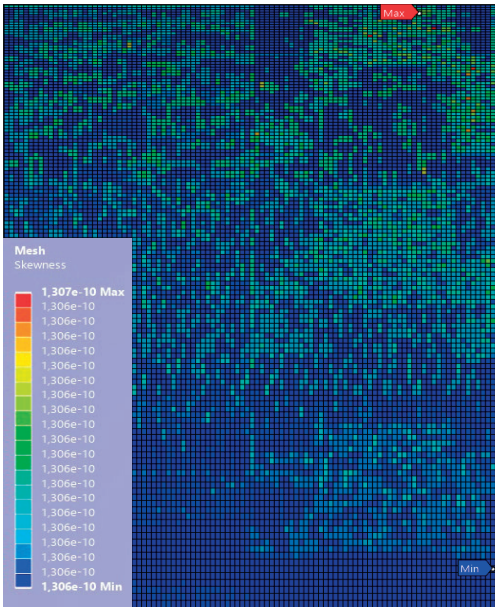


Figure 2. Mesh skewness of the domain

The final computational grid consisted of 14,241 nodes and 14,000 elements, providing an adequate spatial resolution for the numerical simulation of radiation absorption and photochemical degradation processes.

Governing equations

Hydrodynamic behaviour, heat transfer, radiation, and photochemical breakdown of imidacloprid were simulated using computational fluid dynamics (CFD) in ANSYS Fluent.

The model describes the coupled transport of water, heat, radiation and pesticide concentration. The flow of the fluid is described by the *continuity* and *Navier-Stokes equations*:

$$\nabla \cdot \vec{u} = 0$$

$$\rho\left(\frac{\partial \vec{u}}{\partial t} + \vec{u} \cdot \nabla \vec{u}\right) = -\nabla p + \mu \nabla^2 \vec{u} + \rho \vec{g}$$

where $\vec{u}$ is the velocity vector, ρ is the fluid density, p is the pressure, μ is the dynamic viscosity, and $\vec{g}$ is the gravitational acceleration.

Temperature-driven natural convection was modelled with the Boussinesq approximation:

$$\rho = \rho_0[1 - \beta(T - T_{ref})]$$

where ρ_0 is the reference density, β is the thermal expansion coefficient, T is the local temperature, and T_{ref} is the reference temperature.

Heat transfer was described by the energy conservation equation:

$$\rho c_p\left(\frac{\partial T}{\partial t} + \vec{u} \cdot \nabla T\right) = \nabla \cdot (k \nabla T) + S_r$$

where T is the temperature, c_p is the specific heat capacity, k is the thermal conductivity, and S_r is the source term associated with radiation absorption.

Radiative heat transfer in the water was modelled using the Discrete Ordinates (DO) method. The radiative transfer equation is:

$$\vec{s} \cdot \nabla I(\vec{r}, \vec{s}) + (a + \sigma_s) I(\vec{r}, \vec{s}) = a \frac{\sigma T^4}{\pi} + \frac{\sigma_s}{4\pi} \int_{4\pi} I(\vec{r}, \vec{s}') \, d\Omega'$$

where I is the radiation intensity, a is the absorption coefficient of water, σ_s is the scattering coefficient, σ is the Stefan-Boltzmann constant, and $\vec{s}$ is the direction

vector. The absorption coefficient governs the attenuation of radiation in the water column, according to Beer-Lambert's law.
The transport of dissolved imidacloprid in water was described using the species conservation equation:

$$\frac{\partial(\rho Y)}{\partial t} + \nabla \cdot (\rho \vec{u} Y) = \nabla \cdot (\rho D \nabla Y) + R$$

where Y is the mass fraction of imidacloprid, D is the molecular diffusion coefficient in water, and R is the local reaction rate.

Photochemical degradation kinetics
The photochemical degradation of imidacloprid was described using a spatially dependent pseudo-first-order kinetic model implemented via a user-defined function (UDF) in ANSYS Fluent. The local photodegradation rate constant was defined as a function of ultraviolet radiation intensity and temperature.

$$k_{photo}(z,T) = \Phi * \varepsilon_{UV} * I_{UV}(z) * f_T$$

Ultraviolet radiation attenuation within the water column was defined by the Beer–Lambert law, which describes exponential decay of light intensity with depth:

$$I_{UV}(z) = I_0 e^{-\alpha z}$$

where $I_{UV}(z)$ denotes the UV radiation intensity at depth z, I_0 is the incident radiation intensity at the water surface, and α is the extinction coefficient of the medium.
The temperature dependence of the reaction rate was introduced through an Arrhenius-type correction factor.

$$f_T = exp\left[-\frac{E_a}{R}\left(\frac{1}{T} - \frac{1}{T_{ref}}\right)\right]$$

where E_a is the activation energy, R is the universal gas constant, T is the local temperature, and T_{ref} is the reference temperature.
Thus, the overall local photodegradation rate constant can be expressed as:

$$k_{photo}(z,T) = \Phi * \varepsilon_{UV} * I_0 e^{-\alpha z} * exp\left[-\frac{E_a}{R}\left(\frac{1}{T} - \frac{1}{T_{ref}}\right)\right]$$

Within the CFD framework, the degradation of the imidacloprid process was implemented through source terms in the species transport equations. The consumption of imidacloprid was expressed as:

$$S_{imd} = -\rho, Y_{imd,} k_{photo}$$

while the formation of the degradation product was defined as:

$$S_{prod} = \rho, Y_{imd} k_{photo} \left(\frac{MW_{prod}}{MW_{imd}}\right)$$

where ρ is the fluid density, Y_{imd} is the mass fraction of imidacloprid, and MW_{prod} and MW_{imd} are the molecular weights of the degradation product and imidacloprid, respectively.

Boundary and initial conditions
Computational simulations were performed in a two-dimensional water column subjected to ultraviolet irradiation at the free surface. The upper boundary was a radiation inlet that allowed 40 W m^{-2} of ultraviolet radiation into the computational domain (Benitez et al., 2013). The bottom and lateral boundaries were impermeable no-slip walls. The initial velocity was zero to represent quiescent water before irradiation. The fluid temperature started at 293.15 K. Water properties were constant: density 998.2 kg m^{-3}, dynamic viscosity 0.001 Pa s, thermal conductivity 0.6 W m^{-1} K^{-1}, and specific heat capacity 4182 J kg^{-1} K^{-1}. Radiative transfer used the Discrete Ordinates (DO) model with water optical properties set as absorption coefficient 3.0 m^{-1}, scattering coefficient 0.2 m^{-1}, and refractive index 1.33. Initial imidacloprid concentrations (5, 10, and 15 µg/L) were uniformly distributed in the water column. The molecular diffusion coefficient of imidacloprid in water was constant during the simulations.

Photokinetic model parameters
The parameters used in the user-defined function (UDF) to describe the photodegradation kinetics of imidacloprid are summarised in Table 1. The model incorporates attenuation of UV radiation with depth, the quantum yield

of the photochemical reaction, and the temperature dependence of the reaction rate via an Arrhenius relationship (Appendix 1).

Table 1. Photokinetic parameters used in the CFD mode

Parameter	Symbol	Value	Unit	Description
Incident UV intensity	I_0	1.0	–	UV intensity at water surface
Extinction coefficient	α	3.0	m^{-1}	Light attenuation coefficient
Quantum yield	Φ	0.019	–	Efficiency of photochemical reaction
Photokinetic coefficient	$\varepsilon_{UV,}$	6e-5	–	Photochemical proportionality constant
Activation energy	E_a	20000	J mol^{-1}	Activation energy for degradation
Gas constant	R	8.314	J mol^{-1} K^{-1}	Universal gas constant
Reference temperature	T_{ref}	293.15	K	Reference temperature
Water surface height	H_{top}	0.7	m	Position of free surface

Several intermediate variables required for the photochemical degradation model were stored using the User-Defined Memory (UDM) feature in ANSYS Fluent. These variables allow the spatial visualization and post-processing of the photokinetic parameters during the simulation. The UDM locations were used to store the depth relative to the free surface, the local UV radiation intensity calculated using the Beer-Lambert law, and the corresponding local photodegradation rate constant. The stored variables are summarised in Table 2.

Table 2. Photokinetic parameters used in the CFD mode

UDM index	Stored variable	Description
UDM 0	Depth z	Distance from the free surface used in the Beer–Lambert attenuation law
UDM 1	I_{UV}	Local UV radiation intensity in the water column
UDM 2	k_{photo}	Local photodegradation rate constant

The combined use of UDF and UDM functionalities enables the dynamic evaluation of the photodegradation kinetics and allows detailed spatial analysis of UV radiation intensity and reaction rates within the water column.

Numerical setup

Numerical simulations used a pressure-based solver under transient conditions to capture the system's dynamic response and ensure accurate modelling of time-dependent phenomena. The Discrete Ordinates (DO) radiation model represented ultraviolet radiation in the 0.28 ÷ 0.40 μm spectral range, as this range covers both the UVB and UVA regions relevant to the study objectives. The DO model was chosen for its proven effectiveness in resolving directional radiation effects in participating media, as demonstrated in previous research. Simulations used a 60-second time step and 100 iterations per step, parameters selected to balance computational efficiency and solution stability without significant loss of accuracy. The total simulation time of 2,000 steps (120,000 seconds of irradiation) was set to fully observe the cumulative effects of ultraviolet exposure. Pressure-velocity coupling employed the Rhie-Chow momentum interpolation scheme, which helps to prevent pressure-velocity decoupling issues and is recommended for transient flow calculations. Second-order upwind schemes were applied to the momentum, energy, and radiation equations to improve accuracy and minimise numerical diffusion, following best practices in the literature. The wrapped face gradient correction method was used to reconstruct gradients, thereby enhancing the spatial accuracy of variable gradients on non-orthogonal meshes. Convergence was ensured when energy residuals fell below 10^{-6} and other residuals below 10^{-5}, thresholds commonly adopted to confirm reliable, consistent simulation results.

Data processing and analysis

The simulation results were analysed by examining the spatial distribution of ultraviolet radiation and the corresponding variation of imidacloprid concentration within the reactor domain. Particular attention was given to the vertical penetration of radiation through the water column and its influence on photochemical degradation. Concentration fields were evaluated at different simulation times to observe the progressive decrease in imidacloprid concentration during ultraviolet irradiation. Spatial concentration maps were used to identify zones of enhanced degradation associated with higher radiation intensity. The temporal evolution of the average imidacloprid concentration in the reactor was also analysed to quantify the overall degradation behaviour

and assess the efficiency of ultraviolet-induced photodegradation. The numerical model described in the previous section was used to investigate the photochemical degradation of imidacloprid in water under ultraviolet irradiation. The simulation results provide insight into the spatial distribution of ultraviolet radiation within the water column and the corresponding evolution of imidacloprid concentration over time.

RESULTS AND DISCUSSIONS

The results obtained from the CFD simulations are presented and analysed to evaluate the influence of ultraviolet radiation on the degradation behaviour of imidacloprid in water. Particular attention is given to the penetration of ultraviolet radiation into the water column, the spatial distribution of radiation intensity, and the resulting variation in imidacloprid concentration. The analysis focuses on the temporal evolution of pesticide concentration and the identification of regions where photochemical degradation occurs more rapidly due to higher radiation exposure. These results provide insight into the coupled effects of radiation transport and reaction kinetics governing the degradation process.

UV radiation distribution in water

Ultraviolet radiation was simulated within the water domain using the Discrete Ordinates (DO) model. Figure 3 presents the incident radiation intensity within the reactor, measured in $W \cdot m^{-2}$. The highest intensities are observed near the irradiated surface, where incoming UV radiation interacts directly with the water.

As radiation propagates through the water column, its intensity decreases with depth due to absorption by the medium. This pattern follows the Beer-Lambert law, which describes an exponential decrease in intensity through an absorbing medium.

The simulation indicates that radiation intensity decreases from approximately 39 $W \cdot m^{-2}$ at the irradiated boundary to below 5 $W \cdot m^{-2}$ deeper in the domain. The imposed boundary condition for incident radiation was 40 $W \cdot m^{-2}$. However, the contour plot shows nodal or cell-interpolated values calculated by the numerical solver, not the exact boundary condition.

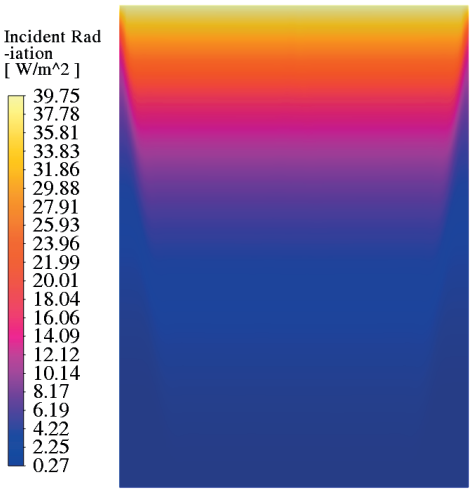


Figure 3. Spatial distribution of incident ultraviolet radiation intensity within the water domain simulated using the Discrete Ordinates radiation model

As a result, the maximum value in the field is slightly lower than the prescribed boundary intensity. In the Discrete Ordinates radiation model in ANSYS Fluent, the radiation intensity field is solved within control volumes. It is then interpolated to nodes for visualisation. The plotted values show the local solution of the radiative transport equation in cells next to the boundary, not the exact boundary input. This explains the small difference between the imposed value (40 $W \cdot m^{-2}$) and the maximum value in the contour plot (≈39 $W \cdot m^{-2}$). Such small deviations are expected in finite-volume discretisation. Here, the radiative flux is evaluated over control-volume faces and distributed across neighbouring cells. So, the slight reduction in the maximum plotted intensity does not mean a physical loss of radiation at the boundary. It simply reflects the numerical representation of the radiation field within the computational mesh.

Temperature evolution during UV irradiation

The thermal response of the water domain under prolonged ultraviolet irradiation was evaluated. Figure 4 presents the spatial distribution of static temperature after 45 hours of continuous UV exposure. The initial water temperature was set at 293.15 K (20°C) to represent typical environmental conditions.

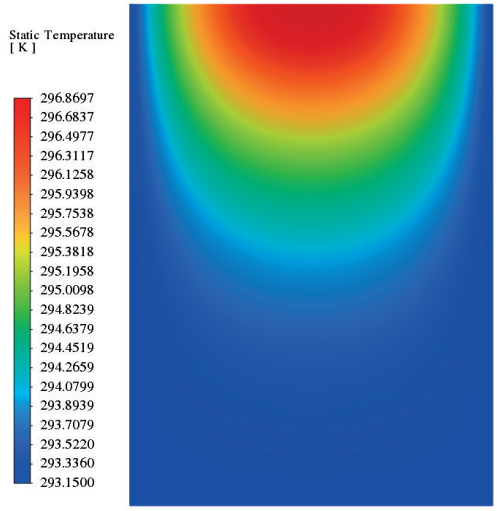


Figure 4. Spatial distribution of temperature in the water domain after 45 hours of ultraviolet irradiation, showing the thermal effect generated by radiation absorption

Simulation results show a gradual increase in temperature within the irradiated region, reaching approximately 296.87 K, a rise of about 3.7 K relative to the initial condition. The observed increase is attributed to the absorption of ultraviolet radiation by water, in which a portion of the radiative energy is converted to thermal energy. The temperature field displays a distinct spatial gradient. The highest temperatures are near the irradiated boundary. This area aligns with the zone of maximum radiation intensity and significant photon energy absorption. As radiation penetrates deeper into the water column, its intensity diminishes due to optical attenuation. This results in reduced local heat generation and lower temperatures. The temperature distribution closely mirrors the spatial pattern of the previously discussed radiation field. This correspondence suggests that the temperature rise is primarily governed by local ultraviolet radiation absorption. Regions exposed to higher photon flux undergo greater radiative heating. Deeper regions remain near the initial temperature due to limited radiation penetration.

Although the overall temperature increase is moderate, the results demonstrate that prolonged ultraviolet irradiation produces measurable thermal effects in the water column. These thermal gradients may influence physicochemical processes such as diffusion rates and reaction kinetics. However, in the present model, the primary factor driving imidacloprid degradation is the availability of ultraviolet photons rather than increased temperature.

Radiation and temperature distributions from simulations reveal the physicochemical conditions that govern imidacloprid degradation in water. The simulated ultraviolet field shows a marked decrease in radiation intensity with increasing depth. This restricts high-energy photons from penetrating the lower regions of the water column. As a result, only the upper portion of the domain receives enough photon flux to initiate photolytic reactions. Inside the water, absorbed radiative power causes a gradual thermal response. This is seen as a temperature increase near the irradiated boundary after extended exposure.

The current model considers photochemical degradation of imidacloprid as a volumetric reaction. The reaction rate depends on local ultraviolet radiation intensity, calculated with the Discrete Ordinates radiation method. Thus, the spatial distribution of radiation intensity directly influences the spatial distribution of the reaction rate. Areas exposed to higher incident radiation are expected to show faster pesticide transformation. Areas with less photon availability become increasingly reaction-limited.

Based on the results, the subsequent section analyses the evolution of imidacloprid concentration within the computational domain, showing how the combined effects of radiation penetration and local energy absorption shape the spatial pattern and temporal progression of pesticide degradation under ultraviolet irradiation.

Spatial distribution of imidacloprid degradation

The spatial distribution of imidacloprid concentration obtained from the CFD simulations is shown in Figure 5. The results illustrate the progressive transformation of the pesticide within the water domain due to ultraviolet irradiation. At the beginning of the simulation, the imidacloprid concentration was uniformly distributed throughout the domain with an initial value of 10 μg/ L. As irradiation

proceeds, the concentration decreases progressively due to radiation-dependent photochemical degradation.

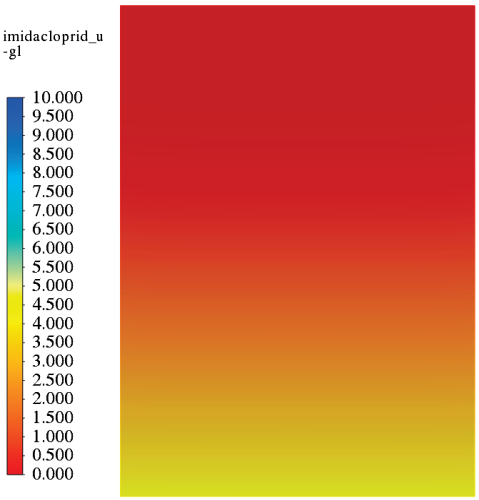


Figure 5. Spatial distribution of imidacloprid concentration within the water domain after UV irradiation

The spatial pattern of imidacloprid concentration corresponds to the distribution of ultraviolet radiation in the water column. Regions close to the irradiated boundary receive the highest radiation intensity and show the largest reduction in pesticide concentration. In contrast, deeper regions retain higher imidacloprid concentrations.

Ultraviolet radiation does not penetrate as deeply due to optical attenuation in water. This result shows that photon availability strongly controls the degradation process. Correspondingly, the complementary distribution of the reaction product formed during the degradation process is presented in Figure 6. As imidacloprid undergoes photochemical transformation, the concentration of the product species increases progressively throughout the domain.

The spatial distribution of the product corresponds to the inverse pattern of the parent compound, with higher product concentrations observed in zones where the degradation of imidacloprid is most pronounced. This complementary behaviour reflects the progressive conversion of the parent pesticide into transformation products as the photochemical reaction proceeds.

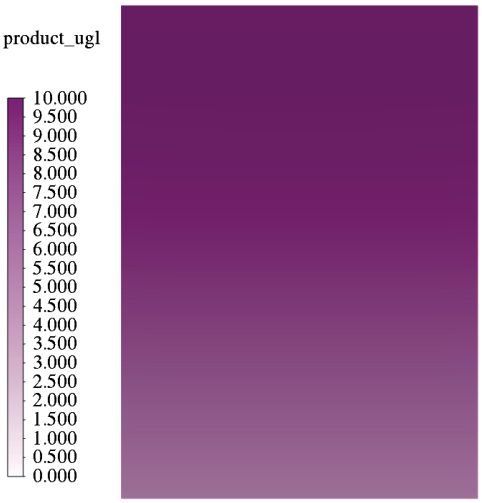


Figure 6. Spatial distribution of the photodegradation product formed during the transformation of imidacloprid

Regions exposed to higher ultraviolet radiation intensities exhibit a faster depletion of the parent compound and, consequently, a higher accumulation of the degradation product. In contrast, areas receiving lower radiation intensities show slower product formation due to the reduced rate of photochemical transformation. This complementary spatial distribution between reactant depletion and product formation confirms the internal consistency of the implemented reaction mechanism within the species transport model and demonstrates that the model adequately captures the mass transfer associated with the photochemical conversion process.

Temporal degradation behaviour and DT_{50}/DT_{90} assessment

To complement the spatial analysis, the temporal evolution of imidacloprid concentration was evaluated for five initial concentration levels: 2.5, 5, 10, 15, and 20 μg L^{-1}. The simulations were performed under identical ultraviolet irradiation and kinetic conditions in order to assess the concentration-dependent response of the degradation process. The resulting concentration profiles are presented in Figure 7.

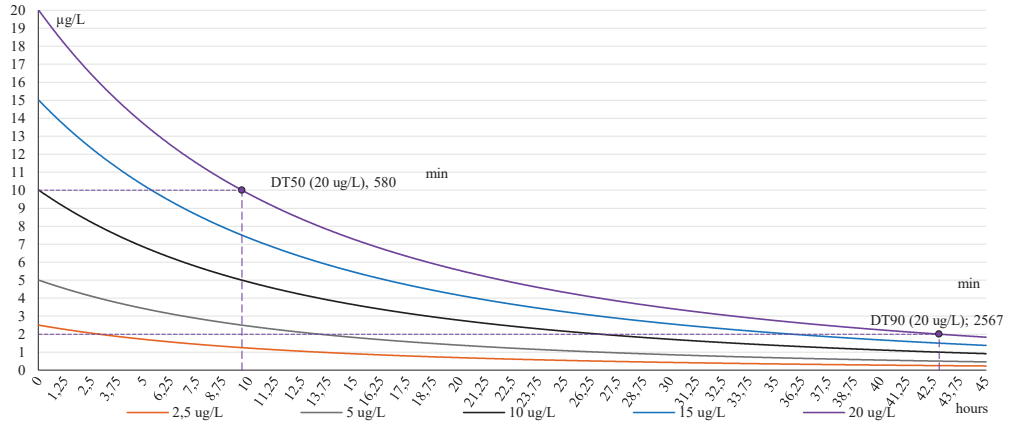


Figure 7. Temporal evolution of imidacloprid concentration during ultraviolet irradiation

The concentration profiles show a continuous decrease in imidacloprid concentration for all investigated initial levels, confirming the progressive degradation of the pesticide under ultraviolet irradiation. The nonlinear decay pattern, characterised by a faster concentration decrease during the initial stage followed by a gradual slowing of the degradation rate, indicates an apparent pseudo-first-order attenuation behaviour.

For the 20 µg L^{-1} scenario, the DT_{50} and DT_{90} values were approximately 580 min and 2567 min, respectively. These values correspond to a decrease in concentration from 20 to 10 µg L^{-1} at DT_{50} and from 20 to approximately 2 µg L^{-1} at DT_{90}. Under the same irradiation and kinetic conditions, the other initial concentrations followed a comparable relative degradation trend. Accordingly, the residual concentrations at DT_{50} were 1.25, 2.5, 5, 7.5, and 10 µg L^{-1}, while at DT_{90} they were approximately 0.25, 0.5, 1.0, 1.5, and 2.0 µg L^{-1} for the initial concentrations of 2.5, 5, 10, 15, and 20 µg L^{-1}, respectively.

Although higher initial concentrations produced larger absolute concentration decreases, the similar shape of the degradation curves indicates that the degradation mechanism remained consistent within the investigated concentration range. This behaviour suggests that imidacloprid attenuation was mainly governed by photon availability and the remaining pesticide concentration, rather than by the initial pollutant loading alone.

Effect of ultraviolet intensity and turbidity on imidacloprid degradation

After establishing the baseline temporal degradation behaviour, additional simulations were performed to evaluate the influence of ultraviolet radiation intensity and attenuation (turbidity) on imidacloprid photodegradation. These parameters directly affect photon availability within the water column and therefore control the spatial and temporal evolution of the degradation process.

The influence of incident ultraviolet radiation intensity on imidacloprid degradation was evaluated by performing additional simulations under otherwise identical model conditions. The temporal concentration profiles presented in Figure 8 were obtained for four radiation intensity levels, namely 20, 30, 40, and 50 W m^{-2}, to assess the sensitivity of the photodegradation process to photon availability.

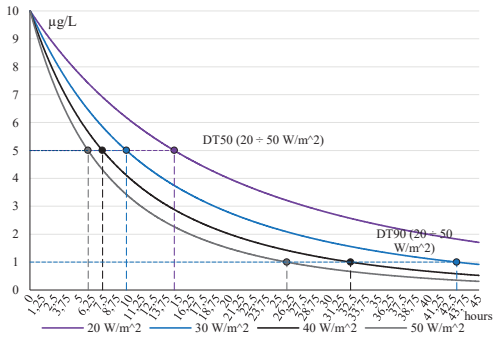


Figure 8. Effect of ultraviolet radiation intensity on the temporal degradation of imidacloprid in water

Higher incident UV irradiance increased photon availability, enhanced the photolytic reaction rate, and shifted the DT_{50} and DT_{90} thresholds toward shorter exposure times. Consequently, the 50 W m^{-2} case showed the highest degradation efficiency, whereas the 20 W m^{-2} case exhibited delayed attenuation, confirming the strong control of radiation intensity on imidacloprid persistence. While higher incident UV irradiance was shown to enhance imidacloprid photodegradation, Figure 9 presents the temporal concentration profiles obtained for different radiation attenuation coefficients.

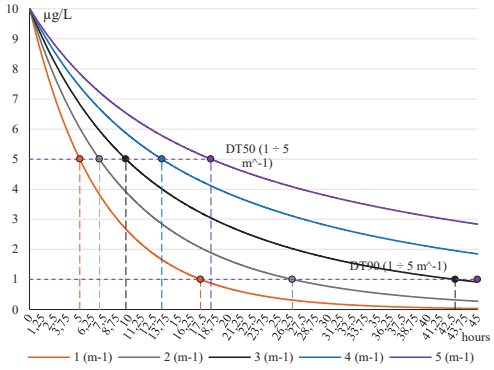


Figure 9. Effect of the radiation attenuation coefficient (turbidity) on the temporal degradation of imidacloprid under UV irradiation

An increase in the attenuation coefficient from 1 to 5 m^{-1} produced a systematic decrease in degradation efficiency, as stronger optical attenuation reduced the UV energy available for photochemical conversion. Consequently, higher turbidity shifted both DT_{50} and DT_{90} toward longer exposure times, confirming that the apparent degradation kinetics are strongly controlled by radiation penetration and photon transport within the aqueous domain.

Model verification and kinetic consistency assessment

The kinetic consistency of the CFD model was assessed by analysing the degradation behaviour of imidacloprid under UV irradiation. Since the implemented reaction mechanism assumed pseudo-first-order photolytic degradation, the temporal evolution of the normalized concentration ratio C/C_0 was examined in semi-logarithmic form. Under pseudo-first-order conditions, the degradation rate is described by:

$$\frac{dC}{dt} = -kC$$

which integrates to:

$$C(t) = C_o e^{-kt}$$

where C is the imidacloprid concentration, C_0 is the initial concentration, and k is the apparent first-order degradation rate constant. As shown in Figure 10, the plot of $\ln(C/C_0)$ versus irradiation time exhibited an approximately linear trend, confirming that the simulated degradation followed pseudo-first-order kinetics.

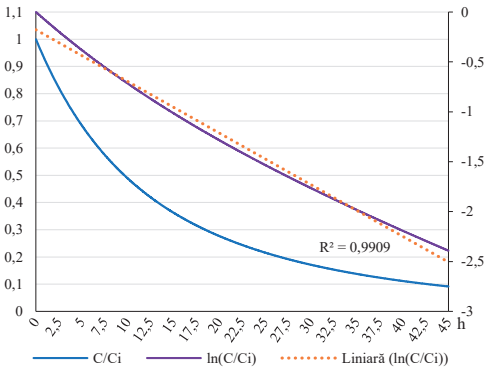


Figure 10. Pseudo-first-order kinetic behaviour of imidacloprid degradation under UV irradiation

The high coefficient of determination, R^2 = 0.9909, indicates good agreement between the numerical results and the assumed kinetic formulation. The apparent degradation rate constant was obtained from the absolute value of the regression slope, while the corresponding half-life was estimated using $t_{1/2}$ = 0.693/k.

To further evaluate model consistency, additional simulations were performed for different initial imidacloprid concentrations under identical UV irradiation and kinetic conditions. The kinetic parameters obtained from these simulations are summarized in Table 3.

Table 3 Summary of simulated kinetic parameters for imidacloprid degradation under different initial concentration, incident UV irradiance, and radiation attenuation conditions

Case	C_0 (μg L^{-1})	UV (W m^{-2})	α (m^{-1})	k (h^{-1})	DT_{50} (h)	DT_{90} (h)	T_{max} (K)	C_{DT90} (μg L^{-1})	Removal (%)	Kinetic behaviour
A1	2.5	40	3	0.0573	12.1	40.2	296.87	0.25	90.0	Pseudo-first-order
A2	5	40	3	0.0573	12.1	40.2	296.87	0.50	90.0	Pseudo-first-order
A3/B3/C3	10	40	3	0.0573	12.1	40.2	296.87	1.00	90.0	Pseudo-first-order
A4	15	40	3	0.0573	12.1	40.2	296.87	1.50	90.0	Pseudo-first-order
A5	20	40	3	0.0573	12.1	40.2	296.87	2.00	90.0	Pseudo-first-order
B1	10	20	3	0.0421	16.5	54.7	296.87	1.00	90.0	Pseudo-first-order
B2	10	30	3	0.0711	9.7	32.4	296.87	1.00	90.0	Pseudo-first-order
B4	10	50	3	0.0849	8.2	27.1	296.87	1.00	90.0	Pseudo-first-order
C1	10	40	1	0.1223	5.7	18.8	296.87	1.00	90.0	Pseudo-first-order
C2	10	40	2	0.0835	8.3	27.6	296.87	1.00	90.0	Pseudo-first-order
C4	10	40	4	0.0414	16.7	55.6	296.87	1.00	90.0	Pseudo-first-order
C5	10	40	5	0.0315	22.0	73.0	296.87	1.00	90.0	Pseudo-first-order

The kinetic parameters summarized in Table 3 show that, under identical irradiation and attenuation conditions, variations in the initial imidacloprid concentration did not modify the apparent degradation rate. For the concentration series, the apparent rate constant remained constant at $k = 0.0573\ h^{-1}$, corresponding to a DT_{50} of 12.1 h and a DT_{90} of 40.2 h. Since C_{DT90} was defined as 10% of the initial concentration, the residual concentration at DT_{90} increased proportionally with C_0, while the characteristic degradation times remained unchanged. This behaviour confirms that the implemented reaction mechanism is consistent with pseudo-first-order photochemical kinetics, for which the apparent rate constant is independent of the initial pollutant concentration under constant irradiation conditions.

In contrast, the simulations performed at different incident UV irradiance levels showed a clear dependence of the degradation kinetics on photon input. Increasing the UV irradiance resulted in higher apparent rate constants and shorter DT_{50} and DT_{90} values, indicating enhanced photolytic degradation due to increased photon availability within the computational domain. Conversely, increasing the radiation attenuation coefficient reduced UV penetration through the water column and led to lower apparent rate constants, thereby delaying both DT_{50} and DT_{90}. This confirms that optical attenuation strongly limits the effective photochemical reaction rate, particularly in regions where the radiation field is reduced by absorption and scattering processes.

The obtained trends are consistent with the expected behaviour of radiation-controlled photochemical degradation in aqueous systems. Previous experimental studies have also reported pseudo-first-order photolysis of imidacloprid under UV irradiation, with faster degradation generally observed under more intense and uniform irradiation conditions (Moza et al., 1998). The comparatively slower degradation predicted in the present CFD simulations can be attributed to the spatially heterogeneous radiation field resolved by the Discrete Ordinates model, which accounts for reduced photon availability within the water depth rather than assuming uniform exposure.

Overall, the kinetic consistency assessment demonstrates that the CFD framework correctly reproduces the main features of pseudo-first-order photodegradation while also capturing the influence of spatially variable UV radiation. The results indicate that imidacloprid persistence in the simulated aquatic domain is governed primarily by photon availability, which is controlled by both incident irradiance and radiation attenuation, whereas the initial pesticide concentration affects the absolute residual concentration but not the apparent degradation rate. These findings provide the basis for the concluding assessment of the model capability to simulate the photochemical fate of pesticides in irradiated aquatic environments.

CONCLUSIONS

This study developed a CFD framework for investigating the photochemical degradation of imidacloprid in water under ultraviolet irradiation. The numerical model coupled UV radiation transport, radiation attenuation, radiation absorption, energy transfer, and reactive species transport, allowing the simulation of photon propagation and its influence on pesticide degradation kinetics.

The results showed that ultraviolet radiation was rapidly attenuated within the water column, generating a pronounced vertical gradient in photon availability. The highest radiation intensity and absorption rates occurred near the irradiated boundary, where UV energy was most available for photochemical transformation. Consequently, imidacloprid degradation was mainly concentrated in the upper irradiated region, while deeper zones exhibited slower transformation rates due to reduced UV penetration. This confirms that radiation attenuation and local photon absorption control the spatial distribution of the photochemical reaction rate.

Under the reference irradiation conditions, the simulated imidacloprid concentration decreased from 10 μg L^{-1} to below 1 μg L^{-1} after 45 h of UV exposure, corresponding to more than 90% removal. The degradation followed pseudo-first-order kinetics, with an apparent rate constant of approximately 0.057 h^{-1} and characteristic degradation times of $DT_{50} \approx 12.1$ h and $DT_{90} \approx 40.2$ h.

The kinetic consistency assessment confirmed that variations in the initial imidacloprid concentration, within the investigated range of 2.5 ÷ 20 μg L^{-1}, did not affect the apparent degradation rate under identical irradiation and radiation attenuation conditions. The residual concentration at DT_{90} increased proportionally with the initial concentration, whereas the rate constant and characteristic degradation times remained unchanged, confirming pseudo-first-order photochemical behaviour.

The sensitivity simulations demonstrated that incident UV irradiance and the radiation attenuation coefficient strongly influence degradation efficiency. Increasing the incident irradiance enhanced photon availability and reduced both DT_{50} and DT_{90} values, while increasing the attenuation coefficient limited UV penetration, decreased the apparent degradation rate, and delayed pesticide transformation. Therefore, both incident UV irradiance and radiation attenuation are key parameters controlling imidacloprid persistence in irradiated aquatic systems.

From an environmental perspective, the findings highlight the relevance of photochemical degradation as a natural attenuation mechanism for pesticides in surface waters. However, the efficiency of this process depends strongly on water depth, optical properties, turbidity-related radiation attenuation, and irradiation conditions, leading to variable pesticide persistence among aquatic environments.

Overall, the proposed CFD framework, coupling the Discrete Ordinates radiation model with UDF-based volumetric reaction terms, provides a useful tool for assessing pesticide photodegradation in aquatic systems by representing UV attenuation, radiation absorption, and reactive contaminant transport. Future work should address experimental validation and model extension toward natural organic matter, suspended solids, and hydrodynamic conditions representative of surface waters.

ACKNOWLEDGEMENTS

The current paper was carried out through the Nucleu Program within the National Research Development and Innovation Plan 2022-2027, carried out with the support of MCID, project no. PN 23 32 01 01, IOSIN PCDIEX.

REFERENCES

Aktar, M. W., Sengupta, D., & Chowdhury, A. (2009). Impact of pesticides use in agriculture: their benefits and hazards. *Interdisciplinary toxicology*, *2*(1). 1–12. https://doi.org/10.2478/v10102-009-0001-7.

Arias-Estévez, M., López-Periago, E., Martínez-Carballo, E., Simal-Gándara, J., Mejuto, J., & García-Río, L. (2008). The mobility and degradation of pesticides in soils and the pollution of groundwater resources. *Agriculture, Ecosystems & Environment*, *123*. 247–260.

Benitez, F. J., Acero, J. L., Real, F. J., Roldan, G. & Rodriguez, E. (2013). Modeling the photodegradation of emerging contaminants in waters by UV radiation

and UV/H_2O_2 system. *Journal of Environmental Science and Health, 48*(1). 120-128.

Blocken, B. (2015). Computational fluid dynamics for urban physics: Importance, scales, possibilities, limitations and ten tips and tricks towards accurate and reliable simulations. *Building and Environment*, 91. 219–245.

Bonmatin, J. M., Giorio, C., Girolami, V., Goulson, D., Kreutzweiser, D. P., Krupke, C., Liess, M., Long, E., Marzaro, M., Mitchell, E. A., Noome, D. A., Simon-Delso, N., & Tapparo, A. (2015). Environmental fate and exposure; neonicotinoids and fipronil. *Environmental science and pollution research international*, *22*(1). 35–67. https://doi.org/10.1007/s11356-014-3332-7.

Chapra, S. C. (1997). *Surface water-quality modeling* (Vol. 1). New York: McGraw-Hill.

Costache, C., & Modrogan, C. (2006). *Ecotoxicology and Risk Assessment*. Bucharest, RO: Agir Publishing House.

European Parliament & Council of the European Union. (2000). Directive 2000/60/EC of the European Parliament and of the Council of 23 October 2000 establishing a framework for Community action in the field of water policy. *Official Journal of the European Communities*, L327. 1–73.

European Parliament & Council of the European Union. (2013). Directive 2013/39/EU of the European Parliament and of the Council of 12 August 2013 amending Directives 2000/60/EC and 2008/105/EC as regards priority substances in the field of water policy. *Official Journal of the European Union*, L226. 1–17.

Fenoll, J., Garrido, I., Hellín, P., & Flores, P. et al., (2011). Photodegradation of neonicotinoid insecticides in water. *Environmental Monitoring and Assessment*, 174. 209–220.

Fischer, H. B., List, E. J., Koh, R. C. Y., Imberger, J., & Brooks, N. H. (1979). *Mixing in inland and coastal waters*. Academic press.

Gavrilescu, M., (2005). Fate of pesticides in the environment and its bioremediation. *Engineering in Life Sciences*, 5(6). 497–526.

Gu, D., Andreev, K., & Dupre, M. E. (2021). Major Trends in Population Growth Around the World. *China CDC weekly*, *3*(28). 604–613. https://doi.org/10.46234/ccdcw2021.160.

Klaassen, C. D., Amdur, M. O., & Doull, J. (1986). *Toxicology – the Basic Science of Poisons 3rd ed*, New York, USA: Macmillan Publishing Company.

Lu, Z., Challis, J. K., & Wong, C.S. (2015). Quantum yields for direct photolysis of neonicotinoid insecticides in water: Implications for exposure to nontarget aquatic organisms. *Environmental Science & Technology Letters, 2*(7). 188–192

Malla, M. A., Gupta, S., Dubey, A., Kumar, A., & Yadav, S. (2021). Contamination of groundwater resources by pesticides. In A. Ahamad, S. I. Siddiqui, & P. Singh (Eds.), *Contamination of Water* . 99–107. Academic Press. https://doi.org/10.1016/B978-0-12-824058-8.00023-2.

Merga, L. B., & Van den Brink, P. J. (2025). A review of climatic zone-related variations in toxicity of imidacloprid towards aquatic species and ecosystems, *Environmental Pollution, 386*(127267). https://doi.org/10.1016/j.envpol.2025.127267.

Moza, P. N., Hustert, K., Feicht, E., & Kettrup, A. (1998). Photolysis of imidacloprid in aqueous solution. *Chemosphere*, 36. 497-502.

Morrissey, C.A., Mineau, P., Devries, J. H., Sanchez-Bayo, F., Liess, M., Cavallaro, M. C., & Liber, K. (2015). Neonicotinoid contamination of global surface waters and associated risk to aquatic invertebrates. *Environment International*, 74. 291–303.

Peterson, C.J. (2007). Imidacloprid mobility and longevity in soil columns at a termiticidal application rate. *Pest management science*, *63*(11). 1124–1132. https://doi.org/10.1002/ps.1433.

Simon-Delso, N., Amaral-Rogers, V., Belzunces, L. P., Bonmatin, J. M., Chagnon, M., Downs, C., Furlan, L., Gibbons, D. W., Giorio, C., Girolami, V., Goulson, D., Kreutzweiser, D. P., Krupke, C. H., Liess, M., Long, E., McField, M., Mineau, P., Mitchell, E. A., Morrissey, C. A., Noome, D. A., & Wiemers, M. (2015). Systemic insecticides (neonicotinoids and fipronil): trends, uses, mode of action and metabolites. *Environmental science and pollution research international*, *22*(1). 5–34. https://doi.org/10.1007/s11356-014-3470-y.

Schwarzenbach, R.P., Gschwend, P.M., Imboden, D.M., (2010). *Environmental Organic Chemistry*, 2nd ed., Wiley.

Stehle, S., Ovcharova, V., Wolfram, J., Bub, S., Herrmann, L. Z., Petschick, L. L., & Schulz, R. (2023). Neonicotinoid insecticides in global agricultural surface waters - Exposure, risks and regulatory challenges. *The Science of the total environment*, *867*. 161383.

Tomizawa, M., & Casida, J. E. (2005). Neonicotinoid insecticide toxicology: mechanisms of selective action. *Annual review of pharmacology and toxicology*, *45*. 247–268.

Tudi, M., Daniel Ruan, H., Wang, L., Lyu, J., Sadler, R., Connell, D., Chu, C., & Phung, D. T. (2021). Agriculture Development, Pesticide Application and Its Impact on the Environment. *International journal of environmental research and public health*, *18*(3). 1112. https://doi.org/10.3390/ijerph18031112.

Van Dijk, T., Van Staalduinen, M., & Van der Sluijs, J., (2013). Macro-invertebrate decline in surface water polluted with imidacloprid. *PLoS ONE*, 8(5). e62374.

Versteeg, H., & Malalasekera, W., (2007). *An Introduction to Computational Fluid Dynamics: The Finite Volume Method.* India: Pearson Education Publishing House.

Wamhoff, H., & Schneider, V., (1999). Photodegradation of imidacloprid. *Journal of Agricultural and Food Chemistry*, 47. 1730–1734.

Wang, H., Wang, F., Yin, S., Liu, S., & Cui, X.-Y. (2026). High-quality quad-dominant mesh generation aided by the virtual topological model generated after automatic suppression of small geometric features. *Computers & Structures, 322*. 108107.

Zhang, Y., Liu, S., Gu, J., Song, F., Yao, X., & Liu, Z. (2008). Imidacloprid acts as an antagonist on insect

nicotinic acetylcholine receptor containing the Y151M mutation. *Neuroscience letters*, *446*(2-3). 97–100.

Zepp, R.G., Hoigné, J., & Bader, H., (1995). Nitrate-induced photooxidation of trace organic chemicals in water. *Environmental Science & Technology*.

Zepp, R. G., Wolfe, N. L., Azarraga, L. V., Cox, R. H. & Pape, C. W. (1977). Photochemical transformation of the DDT and methoxychlor degradation products, DDE and DMDE, by sunlight. *Arch Environ Contam Toxicol* *6*(23). 305–314. https://doi.org/10.1007/BF02097771.

APPENDIX 1

```
#include "udf.h"
#include "math.h"
#define I0        1.0
#define ALPHA     3.0
#define PHI       0.018
#define EPS_UV    0.003
#define EA        20000.0
#define R_GAS     8.314
#define TREF      293.15
#define HTOP      0.7
#define MW_IMD    0.255052
#define MW_PROD   0.255052
#define ID_IMDCPD   0
#define ID_PRODUCT  1
#define ID_WATER    2
#define UDM_DEPTH   0
#define UDM_IUV     1
#define UDM_KPHOTO  2
DEFINE_ADJUST(update_photo_fields, domain)
{
   Thread *t;
   cell_t c;
   real xc[ND_ND];
   real y, z, T;
   real Iuv, fT, k_photo;
   thread_loop_c(t, domain)
   {
      if (!FLUID_THREAD_P(t))
         continue;
      begin_c_loop(c, t)
      {
         C_CENTROID(xc, c, t);
         y = xc[1];
         z = HTOP - y;
         if (z < 0.0)
            z = 0.0;
         T = C_T(c, t);
         if (T < 250.0)
            T = 250.0;
         Iuv = I0 * exp(-ALPHA * z);
         fT = exp(-(EA / R_GAS) * (1.0 / T - 1.0 / TREF));
         k_photo = PHI * EPS_UV * Iuv * fT;
         C_UDMI(c, t, UDM_DEPTH) = z;
         C_UDMI(c, t, UDM_IUV)   = Iuv;
         C_UDMI(c, t, UDM_KPHOTO) = k_photo;
      }
      end_c_loop(c, t)
   }
}
DEFINE_SOURCE(imd_photo_source, c, t, dS, eqn)
{
   real rho, yimd, k_photo, source;
   if (!FLUID_THREAD_P(t))
   {
      dS[eqn] = 0.0;
      return 0.0;
   }
   rho  = C_R(c, t);
   yimd = C_YI(c, t, ID_IMDCPD);
   if (yimd < 0.0)
      yimd = 0.0;
   k_photo = C_UDMI(c, t, UDM_KPHOTO);
   source = -rho * yimd * k_photo;
   dS[eqn] = -rho * k_photo;
   return source;
}
DEFINE_SOURCE(product_photo_source, c, t, dS, eqn)
{
   real rho, yimd, k_photo, source;
   real stoich_mass_ratio;
   if (!FLUID_THREAD_P(t))
   {
      dS[eqn] = 0.0;
      return 0.0;
   }
   rho  = C_R(c, t);
   yimd = C_YI(c, t, ID_IMDCPD);
   if (yimd < 0.0)
      yimd = 0.0;
   k_photo = C_UDMI(c, t, UDM_KPHOTO);
   stoich_mass_ratio = MW_PROD / MW_IMD;
  source = rho * yimd * k_photo * stoich_mass_ratio;
   dS[eqn] = 0.0;
   return                                          source;
```